# The Bandurrias gabbro: Late Oligocene alkaline magmatism in the Patagonian Cordillera

Diego Morata[a,*], Claudia Oliva[a], Rita de la Cruz[b], Manuel Suárez[b]

[a]*Departamento de Geología, Fac. Cs. Físicas y Matemáticas, Universidad de Chile, Plaza Ercilla 803, Santiago, Chile*
[b]*Servicio Nacional de Geología y Minería. Avda, Santa María 0104, Providencia, Santiago, Chile*

**Abstract**

The authors present petrological and geochemical data for the Late Oligocene (ca. 27 Ma) Bandurrias gabbro, a small ($\approx 4.5 \times 3$ km), isolated intrusion near Coyhaique (45°35′ Lat. S), southern Chile, in the present-day backarc region of the Patagonian Cordillera. Its mineral chemistry (olivine, clinopyroxene, feldspars, amphibole, biotite and analcime) is typical of gabbros with alkaline affinity. The development of ophitic and subophitic textures, the extremely elongated acicular apatite crystals, and the low CaO content of olivines (0.17–0.46%), as well as the low $Al^{VI}/Al^{IV}$ ratio (0.00–0.12) of clinopyroxenes, indicate low-pressure (subvolcanic) crystallization conditions. The major, trace, and rare earth element geochemistry also indicate an alkaline affinity ($\Sigma_{alkali} = 4.25$–$7.20\%$, high $TiO_2$ and $P_2O_5$ contents, presence of normative nepheline, $Ti/V > 50$). Geochemical patterns are very similar to those of an ocean island-type alkaline basalt. $(La/Lu)_N$ ratios range from 6.99 to 10.60, and the $Yb_N$ and $Lu_N$ values ($< 10$) suggest the presence of garnet as residual phase in the mantle source. Low Th/La ratios (0.11–0.15) are similar to those of a primitive mantle, and the Zr/Nb (6.3–7.6), La/Nb (0.76–1.03), Ba/Nb (7.6–17.4), Ba/Th (81–120), Th/Nb (0.09–0.15), K/Nb (370–467), Th/La (0.11–0.15), and Ba/La (10.0–16.9) ratios are typical of an enriched mantle-type reservoir. The magma composition suggests generation by low degree partial melting in an extensional or transtensional geodynamic setting. The emplacement of the Bandurrias gabbro took place during a major reconfiguration in the Nazca-South American plate convergence during 28–26 Ma, in either the latest phase of slow, oblique subduction or the subsequent faster, less oblique period of subduction. The data do not allow the authors to rule out either alternative.

*Keywords:* Alkaline magmatism; Late oligocene; Patagonian Cordillera; Transtension

**Resumen**

En el presente trabajo se presentan datos petrológicos y geoquímicos del Gabro Bandurrias (Oligoceno tardío, ca. 27 Ma), una pequeña ($\approx 4{,}5 \times 3$ km) y aislada intrusión cerca de Coyhaique ($\approx 45°35'$ Lat. S), sur de Chile, en la zona de tras-arco de la Cordillera Patagónica. El quimismo de las fases minerales de este gabro (olivino, clinopiroxeno, feldespatos, anfíbol, biotita y analcima) es típico al de gabros con afinidad alcalina. El desarrollo de texturas ofíticas y subofíticas, cristales extremadamente alargados de apatitos, y los bajos contenidos en CaO de los olivinos (0,17–0,46%), así como los bajos valores en la relación $Al^{VI}/Al^{IV}$ (0,00–0,12) en los piroxenos, son indicativos de condiciones de cristalización a baja presión (subvolcánicas). La geoquímica de elementos mayores, trazas y tierras raras de este gabro también indica una afinidad alcalina ($\Sigma_{álcalis} = 4{,}25$–$7{,}20\%$, altos contenidos en $TiO_2$ y $P_2O_5$, presencia de nefelina normativa y valores $Ti/V > 50$), con gran similitud con los patrones de los basaltos tipo islas oceánicas (OIB). Los valores de $(La/Lu)_N$ varían entre 6,99 a 10,60 y los contenidos en $Yb_N$ y $Lu_N$ ($< 10$) indicarían la presencia de granate como fase residual en la fuente mantélica. Los bajos valores de la relación Th/La (0,11–0,15) son similares a los del manto primitivo, y los valores de las relaciones Zr/Nb (6,3–7,6), La/Nb (0,76–1,03), Ba/Nb (7,6–17,4), Ba/Th (81–120), Th/Nb (0,09–0,15), K/Nb (370–467), Th/La (0,11–0,15) y Ba/La (10,0–16,9) son típicas de los de los reservorios tipo EM. El Gabro Bandurrias se habría generado como consecuencia de bajas tasas de fusión parcial parcial y su composición química sugiere un emplazamiento en un ambiente tectónico extensional o transtensional. El Gabro Bandurrias se emplazó durante un

* Corresponding author. Tel.: +56 2 678 4539; fax: +56 2 696 3050.
*E-mail address:* dmorata@cec.uchile.cl (D. Morata).

período de rearreglo mayor de las placas de Nazca y América del Sur (entre los 28–26 Ma), bien durante la última etapa de subducción más lenta y oblicua o durante un período de convergencia más rápida y menos oblicua. Los datos actuales no permiten favorecer ninguna de estas dos alternativas.

*Palabras claves:* Magmatismo alcalino; Oligoceno tardío; Cordillera Patagónica; Transtensión.

## 1. Introduction

Alkaline magmatism is well represented in continental areas that show extensional tectonism (Wilson and Downes, 1991; Wedepohl et al., 1994; Wilson et al., 1995; Griffiths et al., 1997; Dostal and Owen, 1998; Ngounouno et al., 2001), though a gradual transition from orogenic calc-alkaline to continental intraplate alkaline magmatism has been documented in several regions (e.g. Stern et al., 1990; Coulon et al., 2002). In subduction-related regions, alkaline magmatism occurs in the backarc domains and is generally related to an extensional regime that allows mantle upwelling and melt production by a slab rollback (Hole et al., 1995; Haschke et al., 2002).

In the Patagonian Cordillera, alkaline and ocean island basaltic (OIB)-type magmatism is well developed and associated with the Eocene–Pliocene Patagonian flood basalts (Baker et al., 1981; Stern et al., 1990; Demant et al., 1996; Morata et al., 2000; Gorring and Kay, 2001). Pliocene Patagonian flood alkaline basalts have been related to a slab window that formed as a consequence of the subduction of an active ridge (D'Orazio et al., 2001; Gorring and Kay, 2001). Minor alkaline manifestations have been described as Carboniferous metabasites, including pillow basalts in the eastern Andes metamorphic complex (Hervé et al., 1999), and as Late Cretaceous peralkaline plutonic rocks (Welkner et al., 2002). Two small outcrops of Eocene and Mio–Pliocene teschenites have been described by Busteros and Lapido (1983) in the backarc domain of the Patagonian Cordillera, in the hills south of Lago Buenos Aires (Lago General Carrera in Chile, 71°13′W–46°46′S and 71°28′W–4627′S), and related to the Eocene and Mio–Pliocene plateau basalts in the area.

In this article, we present the petrology, mineral chemistry, and whole-rock geochemistry (major, trace, and rare earth elements [REE]) of the Late Oligocene alkaline Bandurrias gabbro, located north of the Lago General Carrera-Buenos Aires at approximately 45°30′S and 71°50′W. We propose a petrogenetic model for this magmatism based on geochemical data. Finally, we discuss the relationship of this outcrop with the Oligocene tectonic evolution of the Patagonian Cordillera.

## 2. Geological context

The evolution of the southern Andean orogen has been marked by the collision of two oceanic ridges with the trench during the past 50 Ma (Cande and Leslie, 1986). During Cenozoic times, the southeast Pacific margin also experienced two intervals of rapid plate convergence: one between 50 and 42 Ma and the other between 25 and 10 Ma (Cande and Leslie, 1986; Pardo-Casas and Molnar, 1987). At approximately 26 Ma, a major readjustment of plates took place from the highly oblique subduction (N10°E) of the Nazca plate under the South American plate at a relatively slow convergence rate ($35 \pm 25$ mm/a) to near-orthogonal convergence (N80°E) at a faster average rate ($112 \pm 8$ mm/a; Cande and Leslie, 1986; Pardo-Casas and Molnar, 1987). Pankhurst et al. (1999), Stern et al. (2000) and Muñoz et al. (2000) show a clear relationship between the changes in the convergence rate and the degree and style of magmatism in southern Chile.

Since the Late Jurassic, eastward subduction of the Pacific oceanic crust under southern South America has taken place and generated the Patagonian batholith and the Meso–Cenozoic volcanic units of the central Patagonian Cordillera (Baker et al., 1981; Weaver et al., 1990; Bruce et al., 1991; Pankhurst et al., 1998; Pankhurst et al., 2000; Suárez et al., 1999; Suárez and de la Cruz, 2001). The north Patagonian batholith (40°–47°S) is composed of Late Jurassic–Late Cretaceous typical metaluminous calc-alkaline, hornblende-biotite granodiorites and tonalites, with small, Late Miocene–Pliocene satellite bodies and gabbro and quartz-gabbros concentrated in the vicinity of the dextral strike-slip Liquiñe-Ofqui fault zone both within (Pankhurst et al., 1999) and east of (Suárez and de la Cruz, 2001) the batholith.

In the backarc domain, Cenozoic magmatism is represented by the Patagonian flood basalts intercalated in Late Oligocene–Early Miocene marine (Guadal Formation) and Late Paleocene–Eocene (Ligorio Márquez and San José Formations) and Late Early Miocene–Early Middle Miocene (Santa Cruz Formation; Niemeyer et al., 1984; Flint et al., 1994; Frassinetti and Covacecich, 1999; Suárez et al., 2000; Flynn et al., 2002; De la Cruz et al., 2003) continental sediments. Minor Mio–Pliocene plutonic intrusions also occur in the backarc region and are interpreted as satellite bodies of the north Patagonian batholith (e.g. El Paso de las Llaves pluton, Vargas and Hervé, 1994; Pankhurst et al., 1999; Suárez and de la Cruz, 2001; Río de Las Nieves Pluton, Morata et al., 2002).

The Meso–Cenozoic geology of the Coyhaique area (45°35′ Lat. S), located in the backarc domain of the Patagonian Cordillera, is characterized by Middle Late Jurassic subaerial acid volcanic rocks of the Ibáñez group

(part of the Chon Aike silicic large igneous province, Pankhurst et al., 1998) overlain by the Early Cretaceous marine beds of the Coyhaique group, which comprises, from base to top, the Toqui, Katterfeld, and Apeleg Formations (Suárez et al., 1996; De la Cruz et al., 2003a). These beds are paraconformably overlain by the Divisadero group, a widespread succession of subaerial volcanic rocks, which in turn is locally overlain with an angular unconformity by Late Cretaceous calc-alkaline volcanic rocks of the El Toro Formation. Late Cretaceous dacitic and andesitic hypabyssal bodies and Eocene basalts and plugs are well exposed in the region. Late Miocene?—Pliocene easterly derived gravels (Galera Formation *s.str.*) and Quaternary glacial, fluvioglacial, and glacilacustrine deposits constitute the youngest successions.

South of the study area, the Late Oligocene–Early Miocene is represented by the marine Guadal Formation (Frassinetti and Covacecich, 1999), widely represented in Chilean and Argentinean Patagonia (see Malumián, 1999).

The Bandurrias gabbro, a small (4.5×3 km), isolated, NE–SW subvolcanic intrusion, elongated roughly parallel to a NE–SW lineament that has been interpreted as the Coyhaique fault (probably of an extensional or transtensional nature; De la Cruz et al., 2003a), is located 10 km east of Coyhaique (Fig. 1) at the margins of Río Coyhaique. This gabbro intrudes the Divisadero group and Apeleg Formation and is covered by Neogene and Quaternary sediments. K–Ar ages of 28.9±1.3, 28.9±1.0, and 27.8±1.6 Ma have been obtained from biotite concentrates of two gabbro samples (Suárez and de la Cruz, 2001). A concordant Ar–Ar weighted mean plateau age of 26.77±0.13 Ma, an inverse isochrone age of 26.88±0.16 Ma, and a total fusion age of 26.67±0.13 Ma confirm its Late Oligocene crystallization age (Suárez and de la Cruz, 2001).

## 3. Petrology

The composition of the small, massive, mesocratic, homogeneous, and slightly layered subvolcanic Bandurrias gabbro ranges from porphyritic microcrystalline microgabbro to medium-grained gabbro. Decimetric, lenticular, leucocratic, coarse-grained (up to 2 cm) pegmatoidal differentiates occur. The main mineral constituents of the gabbro are fresh, subhedral to anhedral, 2–6 mm, colorless to pale pink olivine; zoned and occasionally hour-glass twinned clinopyroxene; and subhedral to anhedral plagioclase in various proportions. Textures range from hypidiomorphic and inequigranular to ophitic. The remaining minerals include subordinate brown biotite, commonly present

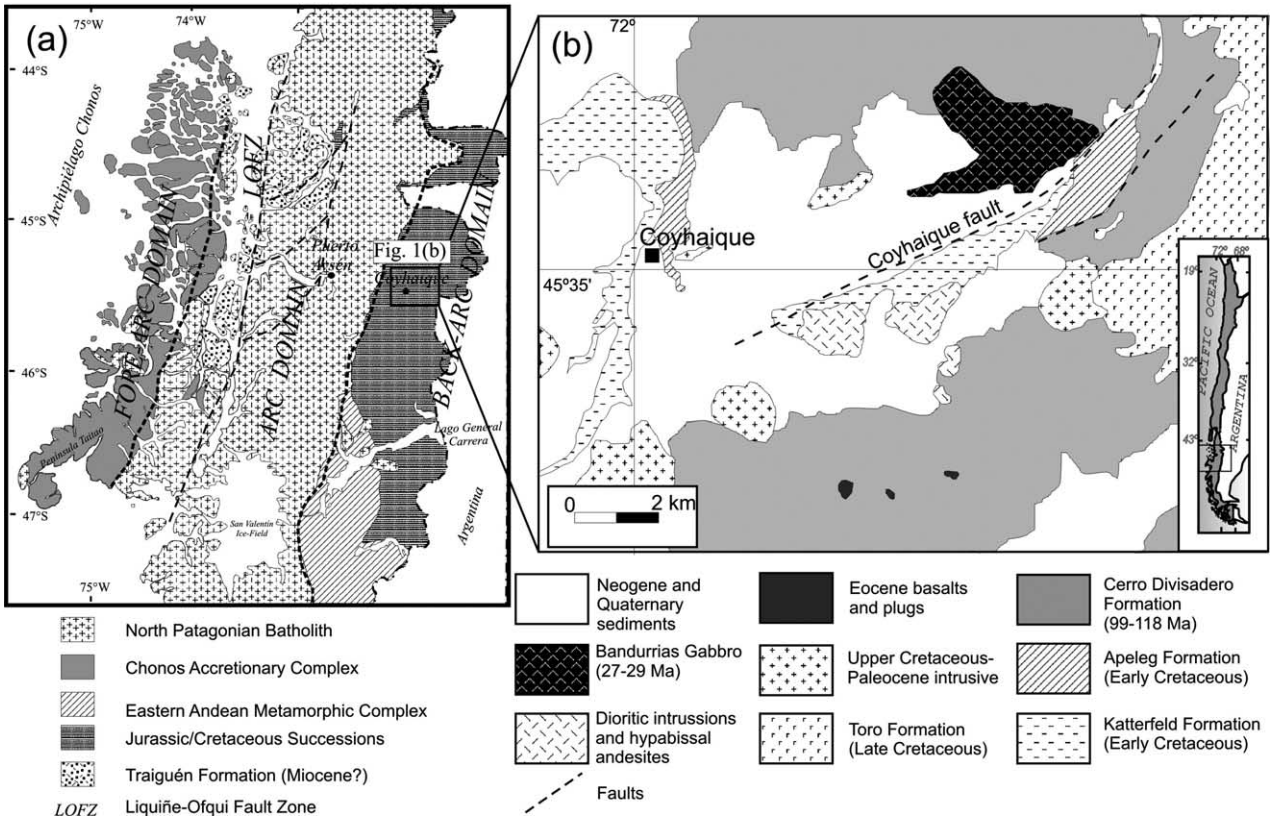


Fig. 1. (a) Simplified geological map of the Patagonian Cordillera between 43°30′ and 47°30′S showing the main geological units (modified from Pankhurst et al., 1999). (b) Sketch of the Bandurrias gabbro in the Patagonian Cordillera (modified from De la Cruz et al., 2003a).

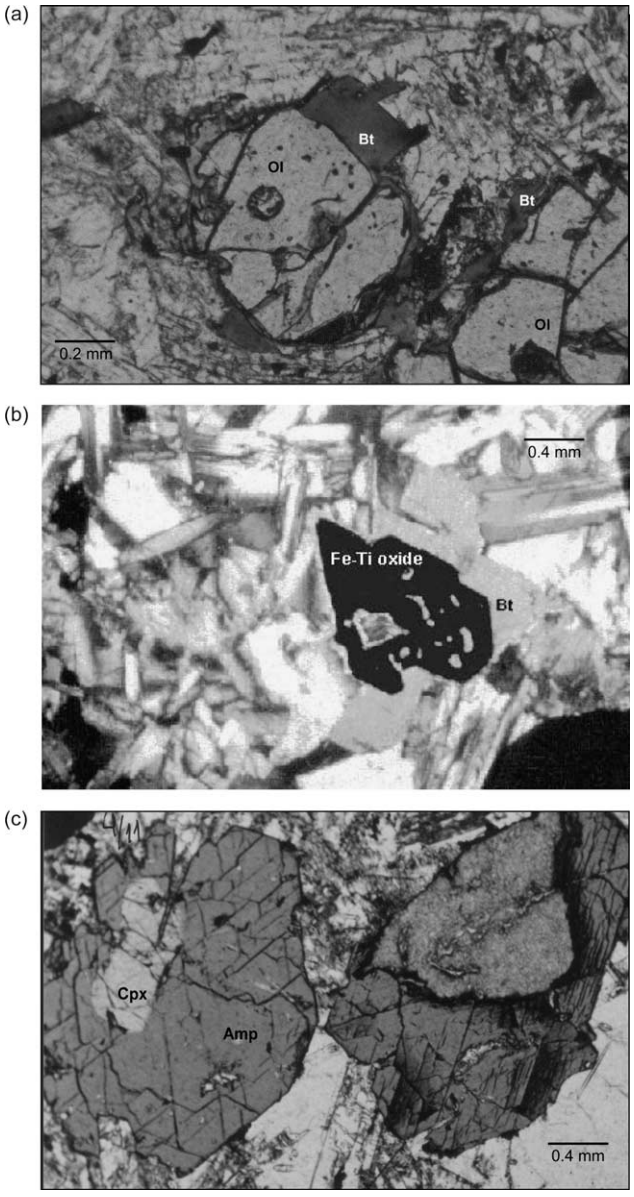


Fig. 2. Thin section photomicrographs of the Bandurrias gabbro showing some of the significant textures. (a) Biotite (Bt) reaction rim around olivine (Ol) crystals in a plagioclase-clinopyroxene intergrown groundmass in sample COY01-6, parallel nicols. (b) Biotite (Bt) rim around a skeletal Fe–Ti oxide in sample COY01-10, crossed nicols. (c) Idiomorphic brown amphibole (Amp) overgrowth clinopyroxene (Cpx), sample COY01-11, crossed nicols.

as reaction rims around olivine (Fig. 2a) and Fe–Ti oxides (Fig. 2b); fine and high acicular apatite; and interstitial analcime. Coarse, idiomorphic (up to 5 mm), pleochroic, reddish-brown, euhedral to subhedral amphibole appears mostly in the lenticular differentiated facies, in which olivine is absent and clinopyroxene is partly surrounded by the amphibole (Fig. 2c). Fine green-rim clinopyroxene, which overgrows the pale pink clinopyroxene, is also present in the most differentiated facies. Only slight secondary alteration is observed as patches of clays and zeolites in some plagioclase crystals. Significant secondary alteration, with intense plagioclase transformation, is observed in the leucocratic pegmatoidal differentiate.

## 4. Mineral chemistry

Mineral analyses were performed with a Cameca SU-30 scanning electron microscope equipped with wavelength and dispersive energy detectors at the Departamento de Geología of the Universidad de Chile (Santiago), with 15 kV, 10 nA, and 10 s as the analytical conditions. The standards were wollastonite for Si and Ca, orthoclase for Al and K, sphene for Ti, diopside for Mg, andradite for Fe, rhodochrosite for Mn, and albite for Na. Full ZAF corrections procedures were applied. Detection limits were approximately 0.1% in weight. Backscattered electron images were obtained using the same Cameca SU-30.

### 4.1. Olivine

Olivine compositions range from $Fo_{74.5}$ at the core to $Fo_{40}$ at the rims of some crystals (Fig. 3). We provide representative analyses in Table 1. CaO ranges from 0.46 to 0.17% without systematic variations, whereas MnO (0.20–1.35%), as we expected, increases with Fe content and reaches the highest values in more fayalitic olivines. The CaO and MnO contents are characteristic of olivine from alkaline series rocks (Ngounouno et al., 2001).

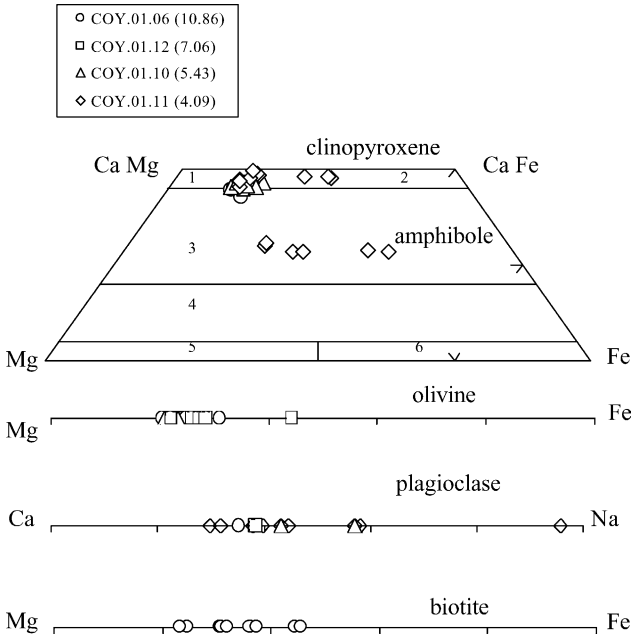


Fig. 3. Compositional variation diagram for the major silicate minerals of the Bandurrias gabbro. In parenthesis, whole-rock MgO wt% content. In the Ca–Mg–Fe triangle, classification of pyroxenes according to Morimoto et al. (1988): 1, diopside; 2, hedenbergite; 3, augite; 4, pigeonite; 5, clinoenstatite; and 6, clinoferrosilite.

Table 1
Representative analyses of olivine from the Bandurrias gabbro

| Sample number | COY.01.06 | COY.01.06 | COY.01.06 | COY.01.10 | COY.01.10 | COY.01.12 | COY.01.12 |
|---|---|---|---|---|---|---|---|
| Analysis | 20 | 21 | 10 | 11 | 24 | 25 | 28 |
| Note | Rim | Core | Core | Core | Rim | Core | Rim |
| $SiO_2$ | 36.21 | 35.37 | 33.95 | 33.10 | 37.66 | 33.64 | 37.66 |
| $TiO_2$ | 0.00 | 0.00 | 0.03 | 0.06 | 0.07 | 0.00 | 0.03 |
| $Al_2O_3$ | 0.06 | 0.03 | 0.06 | 0.02 | 0.05 | 0.01 | 0.02 |
| FeO | 35.79 | 32.98 | 40.45 | 47.84 | 24.01 | 46.49 | 24.35 |
| MnO | 0.73 | 0.60 | 0.75 | 1.35 | 0.49 | 0.79 | 0.20 |
| MgO | 28.19 | 31.63 | 24.63 | 17.89 | 39.35 | 19.79 | 39.01 |
| CaO | 0.17 | 0.36 | 0.36 | 0.39 | 0.36 | 0.46 | 0.41 |
| $Na_2O$ | 0.00 | 0.00 | 0.09 | 0.02 | 0.02 | 0.09 | 0.05 |
| $K_2O$ | 0.00 | 0.00 | 0.00 | 0.00 | 0.00 | 0.02 | 0.00 |
| Sum | 101.15 | 100.97 | 100.32 | 100.68 | 102.00 | 101.30 | 101.74 |
| *Structural formulae calculated to four oxygen* | | | | | | | |
| Si | 0.997 | 0.966 | 0.972 | 0.984 | 0.971 | 0.983 | 0.974 |
| Ti | 0.000 | 0.000 | 0.001 | 0.001 | 0.001 | 0.000 | 0.001 |
| Al | 0.002 | 0.001 | 0.002 | 0.001 | 0.001 | 0.000 | 0.001 |
| Fe | 0.824 | 0.753 | 0.968 | 1.189 | 0.518 | 1.136 | 0.527 |
| Mn | 0.017 | 0.014 | 0.018 | 0.034 | 0.011 | 0.020 | 0.004 |
| Mg | 1.157 | 1.288 | 1.051 | 0.792 | 1.513 | 0.862 | 1.505 |
| Ca | 0.005 | 0.011 | 0.011 | 0.012 | 0.010 | 0.014 | 0.011 |
| Na | 0.000 | 0.000 | 0.005 | 0.001 | 0.001 | 0.005 | 0.000 |
| K | 0.000 | 0.000 | 0.000 | 0.000 | 0.000 | 0.001 | 0.003 |
| Σcation | 3.002 | 3.033 | 3.015 | 3.010 | 3.027 | 3.020 | 3.026 |
| Fo (%) | 58.41 | 63.10 | 66.41 | 52.05 | 39.99 | 74.50 | 74.07 |
| Fa (%) | 41.59 | 36.90 | 33.59 | 47.95 | 60.01 | 25.50 | 25.93 |

### 4.2. Pyroxene

Representative analyses of pyroxenes appear in Table 2. According to Morimoto et al. (1988) classification, all pyroxenes are Ca-rich varieties, major chemical variations are related to the MgO/FeO ratios, and all plotting analyses occur in the diopside-hedenbergite field (Fig. 3). As for the olivines, a correlation is observed between MgO/FeO in pyroxene and that in the host rocks; the MgO-rich pyroxenes occur in the more magnesian host rocks and the FeO-rich pyroxenes in the leucocratic differentiates. Zonation is also observed, ranging in composition from $Wo_{44}Fs_{11}En_{43}$ at the core to $Wo_{47}Fs_{28}En_{23}$ at the rim.

We plot the chemical variation diagrams in Fig. 4, in which four different compositional groups can be observed. Group I is composed of pale pink clinopyroxene, present in all samples, with MgO contents ranging 12.63–15.67 wt%, FeO 7.11–10.02 wt%, $Al_2O_3$ 2.40–4.98 wt%, $Na_2O$ 0.39–0.62 wt%, and $TiO_2$ 1.14–2.12 wt% (Fig. 4). Pyroxenes from group II are characterized by the highest $Al_2O_3$ and $TiO_2$ contents (7–8% and 2.7–3.5%, respectively) and MgO of approximately 13%, with similar $Na_2O$ values to those of group I. Pyroxenes are present in the same crystals as the pyroxene of group I (Fig. 5). Pyroxenes from group III are located at the border of group I (Fig. 5) and characterized by higher aegirine content (10%), higher $Na_2O$ (1.16–1.53%) and FeO (13.21–16.09%), and lower MgO (7.77–9.48%) contents. Finally, group IV is defined by pyroxenes associated with reaction rims in olivine and presents the lowest $Al_2O_3$ (0.59–0.78%) and $TiO_2$ (0.00–0.16%) contents (Fig. 4).

The pyroxene chemical composition ($Al_{tot}/Ti < 10$, low $SiO_2$ content) and variations are typical of pyroxenes from the alkaline series (Le Bas, 1962; Azambre et al., 1992; Chambers and Brown, 1995; Dostal and Owen, 1998).

### 4.3. Feldspars

Feldspars are commonly zoned, and their composition plots in the field of labradorite, ranging from $An_{70}Ab_{29}Or_1$ to $An_{39}Ab_{58}Or_2$ (Table 3, Fig. 6). Plagioclases from the most magnesian samples have the highest anorthite component, which suggests a correlation between the MgO of the host rocks and CaO in plagioclase (Fig. 3). Some plagioclase rims have a more albitic and orthoclase component ($An_{28}Ab_{67}Or_5$) that plots close to the oligoclase-andesine boundary (Fig. 6). In some cases, the plagioclase cores ($An_{42}Ab_{56}Or_2$) are rimmed by orthoclase rims of $An_2Ab_{39}Or_{59}$ (Figs. 6 and 7). In the leucocratic differentiates, rare orthoclase cores ($An_1Ab_{43}Or_{56}$) are present (Fig. 6).

### 4.4. Amphiboles

Only amphiboles from the leucocratic differentiates were analyzed (Fig. 3). In the mesocratic gabbro, amphiboles are minor and always rimming clinopyroxenes (Fig. 2c). According to the classification by Leake et al.

Table 2
Representative analyses of clinopyroxenes from the Bandurrias gabbro

| Sample number | COY.01.06 | COY.01.06 | COY.01.10 | COY.01.10 | COY.01.11 | COY.01.12 | COY.01.12 | COY.01.11 | COY.01.11 | COY.01.11 | COY.01.11 | COY.01.11 | COY.01.11 | COY.01.06 |
|---|---|---|---|---|---|---|---|---|---|---|---|---|---|---|
| Analysis | 11 | 12 | 2 | 3 | 37 | 18 | 19 | 26 | 34 | 36 | 27 | 32 | 38 | 19 |
| Note | Core | Rim | Rim | Core | Core | Core | Rim | Core | Core | Core | Rim | Rim | Rim | rim in Ol. |
| Group | I | I | I | I | I | I | I | II | II | II | III | III | III | IV |
| $SiO_2$ | 51.06 | 51.00 | 48.86 | 51.41 | 48.99 | 51.487 | 50.71 | 44.49 | 46.58 | 45.34 | 50.16 | 49.50 | 48.20 | 54.05 |
| $TiO_2$ | 1.48 | 1.19 | 1.99 | 1.14 | 1.89 | 1.224 | 1.58 | 3.37 | 2.89 | 3.38 | 0.88 | 0.69 | 1.70 | 0.17 |
| $Al_2O_3$ | 3.01 | 3.12 | 4.09 | 3.40 | 4.42 | 2.479 | 2.76 | 8.36 | 7.06 | 7.83 | 2.70 | 1.76 | 3.79 | 0.78 |
| FeO | 7.11 | 7.61 | 9.45 | 7.13 | 8.01 | 8.76 | 9.17 | 8.50 | 8.48 | 7.59 | 13.21 | 16.09 | 15.41 | 8.77 |
| MnO | 0.31 | 0.08 | 0.35 | 0.01 | 0.03 | 0.03 | 0.08 | 0.32 | 0.23 | 0.13 | 0.53 | 0.73 | 0.54 | 0.35 |
| MgO | 15.67 | 15.37 | 13.37 | 15.40 | 14.49 | 14.42 | 14.06 | 12.25 | 12.50 | 12.32 | 9.48 | 7.92 | 7.77 | 15.13 |
| CaO | 22.09 | 22.40 | 21.90 | 22.42 | 21.91 | 21.64 | 22.42 | 22.38 | 22.99 | 22.71 | 22.25 | 22.18 | 21.52 | 21.00 |
| $Na_2O$ | 0.52 | 0.57 | 0.59 | 0.40 | 0.48 | 0.52 | 0.53 | 0.83 | 0.58 | 0.59 | 1.53 | 1.16 | 1.36 | 1.36 |
| $K_2O$ | 0.04 | 0.02 | 0.00 | 0.03 | 0.01 | 0.01 | 0.08 | 0.01 | 0.00 | 0.00 | 0.06 | 16.09 | 0.09 | 0.09 |
| Sum | 101.27 | 101.36 | 100.59 | 101.33 | 100.23 | 100.56 | 101.38 | 100.51 | 101.31 | 99.89 | 100.80 | 100.02 | 100.38 | 101.70 |
| *Structural formulae calculated to six oxygen* | | | | | | | | | | | | | | |
| Si | 1.857 | 1.854 | 1.811 | 1.869 | 1.808 | 1.900 | 1.861 | 1.646 | 1.713 | 1.688 | 1.884 | 1.904 | 1.842 | 1.956 |
| $Al^{IV}$ | 0.129 | 0.133 | 0.179 | 0.131 | 0.192 | 0.100 | 0.119 | 0.354 | 0.287 | 0.312 | 0.116 | 0.080 | 0.158 | 0.033 |
| Ti | 0.040 | 0.032 | 0.055 | 0.031 | 0.052 | 0.034 | 0.044 | 0.094 | 0.080 | 0.095 | 0.025 | 0.020 | 0.049 | 0.005 |
| $Al^{VI}$ | 0.000 | 0.000 | 0.000 | 0.015 | 0.000 | 0.008 | 0.000 | 0.010 | 0.019 | 0.032 | 0.003 | 0.000 | 0.013 | 0.000 |
| $Fe^{3+}$ | 0.115 | 0.135 | 0.130 | 0.083 | 0.121 | 0.061 | 0.112 | 0.217 | 0.148 | 0.132 | 0.177 | 0.158 | 0.153 | 0.145 |
| $Fe^{2+}$ | 0.103 | 0.099 | 0.166 | 0.136 | 0.129 | 0.210 | 0.172 | 0.051 | 0.116 | 0.107 | 0.244 | 0.367 | 0.346 | 0.124 |
| $Mn^{2+}$ | 0.010 | 0.003 | 0.011 | 0.000 | 0.001 | 0.001 | 0.002 | 0.010 | 0.007 | 0.004 | 0.017 | 0.024 | 0.018 | 0.011 |
| Mg | 0.849 | 0.833 | 0.739 | 0.834 | 0.797 | 0.794 | 0.769 | 0.676 | 0.686 | 0.684 | 0.531 | 0.454 | 0.443 | 0.816 |
| Ca | 0.861 | 0.872 | 0.870 | 0.873 | 0.867 | 0.856 | 0.882 | 0.887 | 0.906 | 0.906 | 0.895 | 0.914 | 0.881 | 0.814 |
| Na | 0.037 | 0.040 | 0.042 | 0.028 | 0.035 | 0.037 | 0.038 | 0.060 | 0.041 | 0.042 | 0.111 | 0.086 | 0.101 | 0.095 |
| K | 0.002 | 0.001 | 0.000 | 0.001 | 0.000 | 0.000 | 0.004 | 0.001 | 0.000 | 0.000 | 0.003 | 0.000 | 0.004 | 0.004 |
| Σ cation | 4.002 | 4.003 | 4.003 | 4.002 | 4.003 | 4.001 | 4.003 | 4.005 | 4.003 | 4.003 | 4.006 | 4.007 | 4.006 | 4.003 |
| En (%) | 43.83 | 42.90 | 38.57 | 43.31 | 41.64 | 41.30 | 39.71 | 36.70 | 36.80 | 37.31 | 28.47 | 23.69 | 24.06 | 42.74 |
| Fs (%) | 11.76 | 12.18 | 16.04 | 11.36 | 13.10 | 14.18 | 14.78 | 15.10 | 14.56 | 13.26 | 23.49 | 28.61 | 28.06 | 14.62 |
| Wo (%) | 44.41 | 44.93 | 45.39 | 45.33 | 45.26 | 44.53 | 45.51 | 48.20 | 48.64 | 49.43 | 48.04 | 47.70 | 47.88 | 42.64 |

$Fe^{3+}/Fe^{2+}$ ratio calculated according Droop (1987).

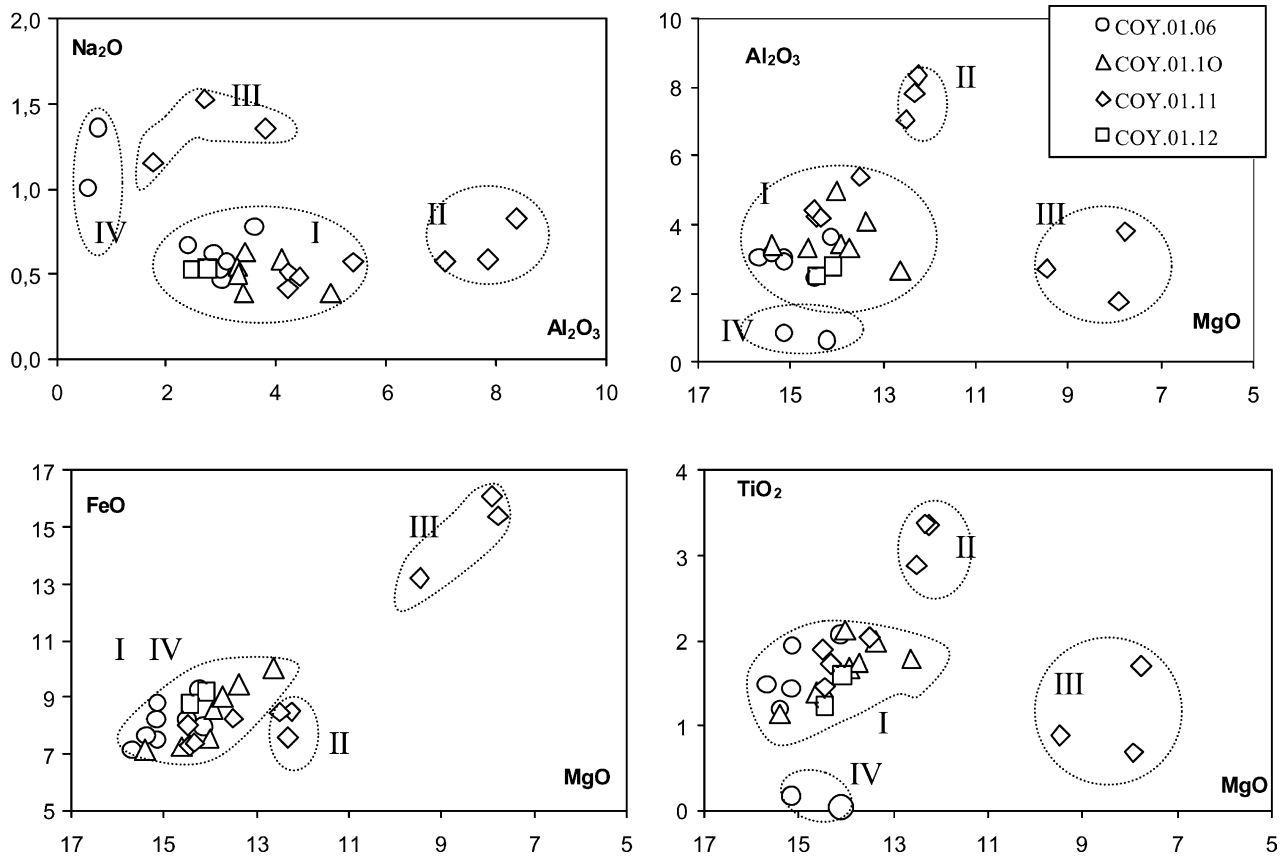


Fig. 4. Pyroxene chemical variations of the four different defined groups. Symbols as in Fig. 2.

(1997), amphiboles (chemical composition in Table 4) mostly plot in the kaersutite and ferrokaersutite fields, with $TiO_2$ ranging from 3.68 to 5.95% and a high aluminium content (2.298–2.692 a.p.f.u.). Three analyses with Ti = 0.414–0.425 (Table 4) plot in the pargasite field. Chemical variations in single crystals are characterized by an increase in FeO from the core (12.22%) to the rim (14.78%) and a decrease in MgO and $TiO_2$. No major chemical differences are observed between idiomorphic amphiboles and amphiboles overgrowing and pseudomorphing clinopyroxenes. Compositionally, these amphiboles resemble those of an alkaline series (Azambre et al., 1992; Dostal and Owen, 1998).

### 4.5. Biotite

Biotite is always accessory (<5% in volume) and appears as reaction rims around olivine (Fig. 2a) and Fe–Ti oxides (Fig. 2b) and as individual, subanhedral crystals, which indicates that it formed at the end of the crystallization when residual liquids were sufficiently enriched in $K_2O$ and $H_2O$ to stabilize it. The $X_{Mg}$ ratio (=Mg/(Mg+Fe)) ranges from 0.40 to 0.65 (Fig. 3) and shows variable $TiO_2$ contents (0.12–6.93%), with $TiO_2$ decreasing as MgO increases. According to the $Al^{IV}$ and Fe/(Fe+Mg) ratios, both types of biotites can be classified as eastonite. Major differences between individual crystals and biotites at the rim are mostly related to the $TiO_2$, FeO, and MgO contents (Table 5); the Ti-rich biotites are those that rim Fe–Ti oxides.

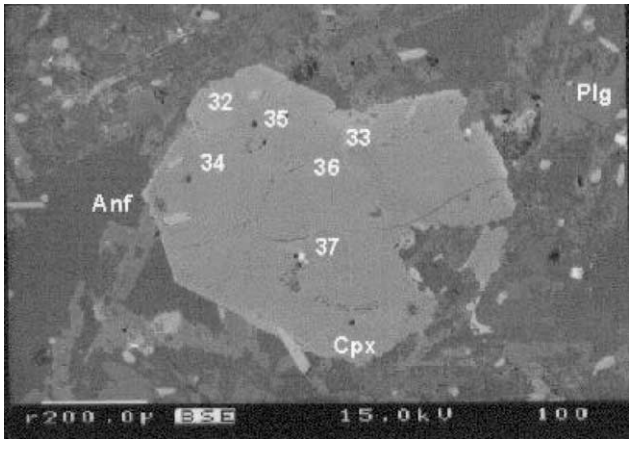


Fig. 5. Electron backscattered image of sample COY01-11 (pegmatoidal differentiate) in which pyroxenes (light gray) from groups I (37) and II (34 and 36) coexist as cores of a same idiomorphic pyroxene crystal. $Na_2O$-rich pyroxenes from group III (32 and 38) are also present in this sample at the rims of the crystals. Numbers indicate microprobe analyses in Table 2. Groundmass is composed of idiomorphic plagioclase (Plg) crystals and interstitial analcime (Anl, dark gray) and small Fe–Ti ores (crystals in white).

Table 3
Representative analyses of feldspars from the Bandurrias gabbro

| Sample number | COY01.06 | COY01.06 | COY01.06 | COY01.06 | COY.01.06 | COY.01.10 | COY.01.10 | COY.01.10 | COY.01.10 | COY.01.10 | COY.01.10 | COY.01.11 | COY.01.11 | COY.01.12 |
|---|---|---|---|---|---|---|---|---|---|---|---|---|---|---|
| Analysis | 2 | 3 | 9 | 16 | 14 | 6 | 8 | 9 | 15 | 16 | 17 | 41 | 45 | 23 |
| Note | Core | Rim | Rim | Core | Core | Core | Core | Rim | Core | Core | Rim | Core | Core | Core |
| $SiO_2$ | 51.85 | 53.69 | 53.83 | 57.44 | 52.54 | 54.79 | 58.79 | 66.81 | 53.86 | 51.28 | 64.75 | 65.79 | 57.49 | 53.19 |
| $TiO_2$ | 0.05 | 0.27 | 0.15 | 0.17 | 0.07 | 0.02 | 0.21 | 0.12 | 0.09 | 0.07 | 0.10 | 0.05 | 0.09 | 0.12 |
| $Al_2O_3$ | 31.38 | 30.70 | 29.84 | 27.17 | 30.08 | 29.58 | 27.27 | 19.59 | 29.55 | 31.83 | 24.03 | 19.02 | 26.89 | 30.36 |
| FeO | 0.18 | 0.19 | 0.23 | 0.38 | 0.40 | 0.03 | 0.24 | 0.08 | 0.28 | 0.17 | 0.09 | 0.23 | 0.25 | 0.18 |
| MnO | 0.01 | 0.01 | 0.04 | 0.04 | 0.03 | 0.00 | 0.00 | 0.12 | 0.04 | 0.04 | 0.01 | 0.00 | 0.06 | 0.08 |
| MgO | 0.01 | 0.01 | 0.00 | 0.00 | 0.00 | 0.00 | 0.01 | 0.00 | 0.00 | 0.00 | 0.00 | 0.00 | 0.00 | 0.00 |
| CaO | 14.60 | 13.42 | 12.44 | 9.28 | 13.09 | 12.02 | 9.07 | 0.35 | 12.02 | 14.51 | 4.52 | 0.23 | 8.51 | 12.27 |
| $Na_2O$ | 3.41 | 4.53 | 3.73 | 7.09 | 4.77 | 5.04 | 6.63 | 4.36 | 5.33 | 3.74 | 6.04 | 4.93 | 6.97 | 4.24 |
| $K_2O$ | 0.20 | 0.15 | 0.03 | 0.28 | 0.18 | 0.19 | 0.45 | 10.11 | 0.18 | 0.11 | 0.68 | 9.85 | 0.43 | 0.18 |
| Sum | 101.67 | 102.97 | 100.29 | 101.84 | 101.15 | 101.68 | 102.66 | 101.53 | 101.34 | 101.73 | 100.22 | 100.10 | 100.68 | 100.61 |
| *Structural formulae calculated to eight oxygen* | | | | | | | | | | | | | | |
| Si | 2.324 | 2.372 | 2.422 | 2.546 | 2.368 | 2.438 | 2.574 | 2.975 | 2.414 | 2.300 | 2.825 | 2.977 | 2.569 | 2.393 |
| Ti | 0.002 | 0.009 | 0.005 | 0.006 | 0.002 | 0.001 | 0.007 | 0.004 | 0.003 | 0.002 | 0.003 | 0.002 | 0.003 | 0.004 |
| Al | 1.658 | 1.598 | 1.582 | 1.419 | 1.598 | 1.551 | 1.407 | 1.028 | 1.561 | 1.683 | 1.236 | 1.015 | 1.416 | 1.610 |
| $Fe^{2+}$ | 0.007 | 0.007 | 0.009 | 0.014 | 0.015 | 0.001 | 0.009 | 0.003 | 0.010 | 0.006 | 0.003 | 0.009 | 0.009 | 0.007 |
| $Mn^{2+}$ | 0.000 | 0.000 | 0.001 | 0.001 | 0.001 | 0.000 | 0.000 | 0.005 | 0.001 | 0.001 | 0.000 | 0.000 | 0.002 | 0.003 |
| Mg | 0.001 | 0.001 | 0.000 | 0.000 | 0.000 | 0.000 | 0.000 | 0.000 | 0.000 | 0.000 | 0.000 | 0.000 | 0.000 | 0.000 |
| Ca | 0.701 | 0.635 | 0.599 | 0.441 | 0.632 | 0.573 | 0.425 | 0.017 | 0.577 | 0.697 | 0.211 | 0.011 | 0.408 | 0.592 |
| Na | 0.296 | 0.388 | 0.325 | 0.609 | 0.417 | 0.435 | 0.563 | 0.376 | 0.463 | 0.325 | 0.511 | 0.433 | 0.604 | 0.370 |
| K | 0.011 | 0.008 | 0.002 | 0.016 | 0.010 | 0.011 | 0.025 | 0.574 | 0.010 | 0.006 | 0.038 | 0.569 | 0.024 | 0.011 |
| Σ cation | 4.999 | 5.018 | 4.946 | 5.051 | 5.044 | 5.009 | 5.010 | 4.982 | 5.040 | 5.022 | 4.828 | 5.015 | 5.035 | 4.988 |
| An (%) | 69.50 | 61.59 | 64.69 | 41.39 | 59.69 | 56.22 | 41.98 | 1.73 | 54.93 | 67.78 | 27.83 | 1.11 | 39.35 | 60.88 |
| Ab (%) | 29.37 | 37.60 | 35.10 | 57.15 | 39.34 | 42.71 | 55.55 | 38.89 | 44.12 | 31.64 | 67.19 | 42.73 | 58.31 | 38.04 |
| Or (%) | 1.13 | 0.81 | 0.20 | 1.46 | 0.98 | 1.07 | 2.47 | 59.38 | 0.95 | 0.58 | 4.98 | 56.17 | 2.34 | 1.08 |

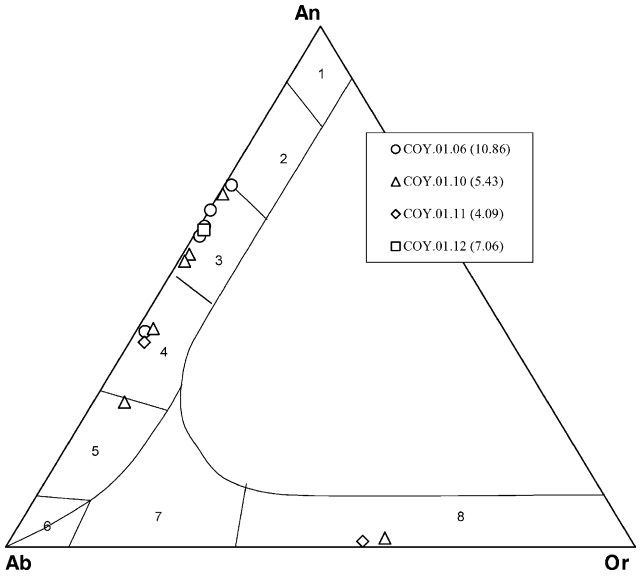


Fig. 6. Feldspar composition plotted in an An:Ab:Or diagram. 1, anorthite; 2, bytownite; 3, labradorite; 4, andesine; 5, oligoclase; 6, albite; 7, anorthoclase; and 8, sanidine. Symbols as in Fig. 2.

### 4.6. Analcime

Analcime occurs as an interstitial (secondary?) phase in the groundmass (Fig. 5) and more abundantly in the leucocratic differentiated pegmatoids. We report the chemical analyses in Table 6; the oxides sum are in the range 88.21–93.14%. There is a decrease in the $Na_2O$ (from 7.61 to 14.53%) and $K_2O$ (from 0.05 to 0.63%) contents with increasing $Al_2O_3$. The highest $Na_2O$ values are observed in analcimes from the leucocratic differentiated variety (sample COY.01.11), whereas analcimes from the mesocratic gabbros have the lowest $Na_2O$ contents and total oxides. This finding may be related to a very slight alteration of analcimes in this last facies or a consequence of variation due to differentiation. The Si/Al ratios range between 1.69 and 2.05. The presence of analcimes and the composition are typical of alkaline magmas (Dostal and Owen, 1998); its origin may be interpreted as a primary or alteration product from a previous Na-rich feldspathoid (e.g. Morata and Higueras, 1996).

## 5. Geochemistry

Five selected samples were analyzed for major, trace, and REE by inductively coupled plasma atomic emission spectrometer (Perkim Elmer 400) at the Departamento de Geología, Universidad de Chile (J. Martínez, analyst). Detection limits were 0.1% for major elements; 2 ppm for Th and Nb; 1 ppm for Ba, Sr, Zr, Y, Cr, V, Ni, Co, Sc, Cu, Zn, Hf, La, Ce, Nd, and Sm; 0.1 ppm for Eu, Gd, Dy, Ho, Er, and Yb; and 0.05 ppm for Lu. The standards were basalt BCR-2, andesite AGV-2, and granite G-2 from US Geological Survey reference materials.

All analyzed samples (Table 7) are characterized by low $SiO_2$ contents (45.03–47.62%) and medium to high values of MgO (4.09–10.86%), $TiO_2$ (1.79–2.68%), CaO (8.53–10.41%), $P_2O5$ (0.40–0.87%), $K_2O$ (0.92–1.88%), and $Na_2O$ (3.33–5.32%). A negative correlation is observed between MgO and $P_2O_5$, $Na_2O$, $K_2O$, and $TiO_2$. $Al_2O_3$ contents are in the interval 14.16–17.20%, and $CaO/Al_2O_3$ ratios range between 0.53 and 0.63. Low loss on ignition (LOI) values (0.95–1.79%) characterize these rocks, and a higher LOI value (4.45%) is detected only in the differentiated leucocratic gabbro from the abundant amphibole as phenocrysts. In comparison with other Tertiary gabbros from the north Patagonian batholith (Table 7), the Bandurrias gabbro has low $SiO_2$ values and high MgO, $TiO_2$, and $P_2O_5$ contents.

According to the total alkali content ($\Sigma_{alkali}$ = 4.25–7.20%), the rocks can be classified as alkaline gabbros with a positive correlation between the $SiO_2$ content and the alkalis. All samples have normative nepheline (8.43–14.03%) and higher content in the leucocratic differentiates, which, with the high $TiO_2$ and $P_2O_5$ values, confirms the gabbro's alkaline character.

Incompatible trace elements (light LREE, Zr, Nb, Y, Ba, and Sr) are relatively enriched and show negative correlation with MgO (Table 7, Fig. 8). The Ti/V ratios are always >50, which is characteristic of alkaline magmatism (Shervais, 1982). In a primitive-mantle normalized trace element diagram (Fig. 8), the Bandurrias gabbro shows similar patterns to those of OIBs and no negative Nb anomaly, which indicates subduction-related rocks, including calc-alkaline lamprohyres. In a La/Nb versus Zr/Nb diagram (not shown), the Bandurrias gabbro shows low values for these ratios, which indicates alkalinity, in comparison with the calc-alkaline granitoids of the northern Patagonian batholith (data from Pankhurst et al., 1999) and gabbros from the satellite Paso de las Llaves pluton (10 Ma, Vargas and Hervé, 1994).

The chondrite-normalized REE diagram (Fig. 9) shows a parallel pattern for all samples, with slightly higher

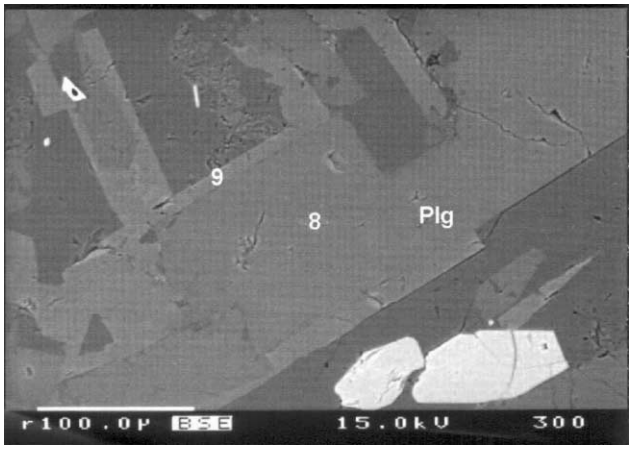


Fig. 7. Electron backscattered image of sample COY01-10 in which a core of anorthictic rich-plagioclase (8) is rimmed by an orthoclase-rich feldspar (9). Numbers indicate microprobe analyses in Table 3.

Table 4
Representative analyses of amphiboles from the Bandurrias gabbro

| Sample number | COY.01.11 | COY.01.11 | COY.01.11 | COY.01.11 | COY.01.11 | COY.01.11 | COY.01.11 |
|---|---|---|---|---|---|---|---|
| Analysis | 22 | 8 | 24 | 28 | 32 | 33 | 43 |
| Note | Core | rim/px | Green rim | Rim/px | Rim | Rim | Rim/px |
| $SiO_2$ | 39.90 | 41.30 | 39.48 | 41.30 | 40.41 | 39.74 | 39.77 |
| $TiO_2$ | 5.95 | 3.68 | 4.70 | 3.68 | 3.77 | 4.52 | 5.56 |
| $Al_2O_3$ | 12.41 | 10.89 | 10.47 | 10.89 | 11.78 | 11.45 | 12.77 |
| FeO | 12.22 | 14.78 | 22.41 | 14.78 | 16.02 | 20.95 | 12.25 |
| MnO | 0.16 | 0.47 | 0.51 | 0.469 | 0.36 | 0.40 | 0.23 |
| MgO | 12.68 | 11.58 | 6.30 | 11.58 | 11.18 | 7.44 | 12.80 |
| CaO | 11.80 | 11.33 | 10.82 | 11.33 | 11.43 | 11.31 | 12.27 |
| $Na_2O$ | 3.03 | 3.53 | 3.24 | 3.53 | 2.92 | 3.17 | 3.07 |
| $K_2O$ | 0.92 | 1.15 | 1.44 | 1.15 | 1.06 | 1.63 | 0.90 |
| Sum | 99.07 | 98.71 | 99.35 | 98.70 | 98.94 | 100.61 | 99.62 |
| *Structural formulae calculated to 23 oxygen* | | | | | | | |
| Si | 6.177 | 5.878 | 6.116 | 6.177 | 6.004 | 5.869 | 6.177 |
| Ti | 0.414 | 0.659 | 0.547 | 0.414 | 0.421 | 0.529 | 0.414 |
| $Al^{IV}$ | 1.823 | 2.122 | 1.884 | 1.823 | 1.996 | 2.101 | 1.823 |
| $Al^{VI}$ | 0.098 | 0.033 | 0.029 | 0.098 | 0.068 | 0.000 | 0.098 |
| $Fe^{2+}$ | 1.825 | 1.499 | 2.903 | 1.824 | 1.587 | 2.671 | 1.825 |
| $Fe^{3+}$ | 0.024 | 0.006 | 0.000 | 0.024 | 0.403 | 0.024 | 0.024 |
| Mn | 0.059 | 0.02 | 0.066 | 0.059 | 0.046 | 0.052 | 0.059 |
| Mg | 2.58 | 2.783 | 1.454 | 2.581 | 2.476 | 1.724 | 2.58 |
| Ca | 1.816 | 1.863 | 1.795 | 1.816 | 1.820 | 1.884 | 1.816 |
| Na | 1.024 | 0.867 | 0.974 | 1.024 | 0.841 | 0.957 | 1.024 |
| K | 0.219 | 0.173 | 0.284 | 0.219 | 0.201 | 0.323 | 0.219 |
| $\Sigma$ cation | 16.058 | 15.903 | 16.053 | 16.059 | 15.863 | 16.164 | 16.058 |

Structural formulae calculated to 13-CNK, using AMPHIBOL software (Richard and Clarke, 1990).

normalized values in the leucocratic differentiated pegmatoids. As Fig. 8 shows, the REE patterns of the Bandurrias gabbro are similar to those of the alkaline OIB. The $Yb_N$ and $Lu_N$ values ($<10$) may indicate the presence of garnet as residual phase in the mantle source. $(La/Lu)_N$ ratios range from 6.99 to 10.60, and no Eu anomaly is observed.

## 6. Discussion and conclusions

The Bandurrias gabbro has some notable differences in timing, location, and geochemistry with relation to the gabbros of the north Patagonian batholith. First, it represents the only Late–Early Oligocene magmatism known in the region between 44° and 49°S (Suárez and de la Cruz, 2001). Second, its location, approximately 200 km east of the axis of the north Patagonian batholith, makes it unique in the Cenozoic magmatic evolution of the central Patagonian Cordillera. Third, it has an alkaline affinity, as is evidenced by its mineral and whole-rock chemistry.

### 6.1. Conditions of emplacement and crystallization

Textures observed in the Bandurrias gabbro, such as the development of ophitic and subophitic textures and acicular extremely elongated apatite crystals, indicate subvolcanic emplacement. This indication is supported by the low CaO (average 0.31%) content in olivines (Brown, 1982) and the low $Al^{VI}/Al^{IV}$ (0.00–0.12) in pyroxenes (Green and Ringwood, 1968), which are typical of low-pressure crystallization conditions.

The presence of two types of pyroxene cores with notable $Al_2O_3$ differences in the pegmatoidal differentiates (Figs. 4 and 5) but no differences in the $Al^{VI}/Al^{IV}$ ratios excludes the possibility of polybaric crystallization. However, pyroxenes of group II are characterized by higher $Al_2O_3$ and $TiO_2$ and lower $SiO_2$ contents. These chemical characteristics reflect the geochemistry of melts from which clinopyroxene could be crystallized and thereby indicate a kind of hybridization of two different melts with different $SiO_2$ undersaturation degrees and $TiO_2$ and $Al_2O_3$ contents. The increase in $TiO_2$ and decrease in $SiO_2$ in this pegmatoidal differentiate occurred as a consequence of the previous crystallization of anhydrous, $TiO_2$-poor silicate phases (olivine, plagioclase, and clinopyroxene), thereby decreasing the $a_{SiO2}$ (which favored the crystallization of analcime) and increasing the $TiO_2$ and $a_{H2O}$ (which favored the formation of the idiomorphic, Ti-rich amphiboles). The presence of centimetric, lenticular pegmatoids imply an in situ differentiation characterized by higher proportions of hydrated phases and a general increase in large ion lithophile elements (LILE), high-field strong elements (HFSE) (Fig. 8), and REE (Fig. 9).

Table 5
Representative analyses of biotites from the Bandurrias gabbro

| Sample number | COY.01.06 | COY.01.06 | COY.01.06 | COY.01.06 | COY.01.06 | COY.01.06 | COY.01.06 | COY.01.10 | COY.01.10 | COY.01.10 |
|---|---|---|---|---|---|---|---|---|---|---|
| Analysis | 6 | 10 | 13 | 19 | 8 | 10 | 21 | 12 | 26 | 27 |
| Note | reaction rim-Ol | reaction rim-Ol | reaction rim-Ol | reaction rim-Ol-ore | rim-Ol | rim-ore | rim-ore | rim-Ol | rim-Ol | rim-Ol |
| $SiO_2$ | 40.82 | 41.11 | 41.13 | 38.62 | 37.47 | 37.91 | 36.93 | 35.96 | 36.63 | 35.96 |
| $TiO_2$ | 0.26 | 0.52 | 0.33 | 3.96 | 6.637 | 4.17 | 6.93 | 1.92 | 0.08 | 0.12 |
| $Al_2O_3$ | 14.91 | 13.63 | 13.73 | 14.07 | 13.57 | 14.19 | 13.98 | 14.25 | 15.15 | 14.00 |
| FeO | 14.35 | 11.81 | 11.57 | 13.69 | 13.93 | 14.21 | 14.80 | 19.51 | 17.28 | 20.48 |
| MnO | 0.16 | 0.02 | 0.01 | 0.00 | 0.00 | 0.21 | 0.17 | 0.21 | 0.30 | 0.15 |
| MgO | 18.28 | 20.45 | 21.56 | 17.16 | 16.72 | 16.99 | 14.69 | 13.66 | 16.32 | 13.71 |
| CaO | 0.13 | 0.09 | 0.03 | 0.19 | 0.18 | 0.10 | 0.00 | 0.00 | 0.33 | 0.24 |
| $Na_2O$ | 0.20 | 0.38 | 0.60 | 0.69 | 1.16 | 1.26 | 0.78 | 0.54 | 0.59 | 0.86 |
| $K_2O$ | 7.20 | 9.18 | 6.28 | 8.68 | 9.13 | 9.62 | 8.77 | 9.51 | 9.11 | 8.85 |
| Sum | 96.30 | 97.18 | 95.23 | 97.04 | 98.80 | 98.69 | 97.05 | 95.54 | 95.79 | 94.36 |
| *Structural formulae calculated to 22 oxygen* | | | | | | | | | | |
| Si | 5.882 | 5.881 | 5.896 | 5.608 | 5.401 | 5.485 | 5.425 | 5.516 | 5.522 | 5.601 |
| Ti | 0.028 | 0.056 | 0.036 | 0.432 | 0.719 | 0.454 | 0.766 | 0.221 | 0.009 | 0.013 |
| Al | 2.532 | 2.298 | 2.319 | 2.409 | 2.305 | 2.419 | 2.419 | 2.575 | 2.692 | 2.569 |
| Fe | 1.729 | 1.412 | 1.387 | 1.662 | 1.680 | 1.720 | 1.818 | 2.502 | 2.178 | 2.667 |
| Mn | 0.020 | 0.002 | 0.001 | 0.000 | 0.000 | 0.026 | 0.021 | 0.027 | 0.039 | 0.019 |
| Mg | 3.925 | 4.361 | 4.607 | 3.715 | 3.592 | 3.664 | 3.217 | 3.123 | 3.667 | 3.182 |
| Ca | 0.020 | 0.014 | 0.005 | 0.029 | 0.027 | 0.015 | 0.000 | 0.000 | 0.053 | 0.040 |
| Na | 0.056 | 0.105 | 0.166 | 0.193 | 0.325 | 0.355 | 0.222 | 0.159 | 0.172 | 0.259 |
| K | 1.323 | 1.676 | 1.149 | 1.607 | 1.680 | 1.776 | 1.643 | 1.861 | 1.753 | 1.758 |
| $\Sigma$ cations | 15.514 | 15.804 | 15.566 | 15.656 | 15.729 | 15.916 | 15.532 | 15.985 | 16.085 | 16.110 |

Table 6
Representative analyses of analcimes from the Bandurrias gabbro

| Sample number | COY01.06 | COY01.06 | COY.01.06 | COY.01.11 | COY.01.11 |
|---|---|---|---|---|---|
| Analysis | 14 | 15 | 15 | 29 | 25 |
| Note | Core | Core | Core | Core | Core |
| $SiO_2$ | 50.35 | 51.69 | 51.39 | 54.86 | 54.98 |
| $TiO_2$ | 0.12 | 0.00 | 0.07 | 0.00 | 0.00 |
| $Al_2O_3$ | 24.81 | 25.88 | 25.59 | 23.01 | 22.73 |
| FeO | 0.09 | 0.00 | 0.00 | 0.00 | 0.00 |
| MnO | 0.01 | 0.08 | 0.00 | 0.00 | 0.05 |
| MgO | 0.00 | 0.01 | 0.00 | 0.01 | 0.03 |
| CaO | 2.91 | 2.59 | 2.91 | 0.67 | 0.71 |
| $Na_2O$ | 10.62 | 7.88 | 7.61 | 14.53 | 14.43 |
| $K_2O$ | 0.33 | 0.42 | 0.63 | 0.05 | 0.09 |
| Sum | 89.24 | 88.54 | 88.21 | 93.14 | 93.01 |
| *Structural formulae calculated to six oxygen* | | | | | |
| Si | 1.907 | 1.940 | 1.939 | 1.992 | 1.999 |
| Ti | 0.003 | 0.000 | 0.002 | 0.000 | 0.000 |
| Al | 1.107 | 1.145 | 1.138 | 0.985 | 0.974 |
| $Fe^{3+}$ | 0.003 | 0.000 | 0.000 | 0.000 | 0.000 |
| $Mn^{2+}$ | 0.000 | 0.002 | 0.000 | 0.000 | 0.001 |
| Mg | 0.000 | 0.001 | 0.000 | 0.001 | 0.002 |
| Ca | 0.118 | 0.104 | 0.118 | 0.026 | 0.028 |
| Na | 0.779 | 0.573 | 0.557 | 1.023 | 1.017 |
| K | 0.016 | 0.020 | 0.031 | 0.002 | 0.004 |
| $\Sigma$ cation | 3.934 | 3.785 | 3.784 | 4.029 | 4.025 |

### 6.2. Source composition

The primitive-mantle normalized multielement diagram (Fig. 8) of the Bandurrias gabbro shows a pattern of LILE and HFSE contents typical of OIB magmas generated in an intraplate setting. The absence of a negative Nb anomaly (Fig. 8) argues against significant crustal contamination. However, the $Yb_N$ values $<10$ (Fig. 9) are compatible with the presence of garnet as a residual phase in the mantle source. According to Weaver (1991), three different mantle end-member sources can be distinguished in the genesis of OIB-type magmas: (1) the HIMU (high $^{238}U/^{204}Pb$, low LILE/HFSE and La/HFSE ratios), compatible with derivation from an ancient oceanic crustal source dehydrated in a subduction zone and recycled into the mantle; (2) the enriched mantle I (EM-I, with higher LILE/HFSE and LREE/HFSE ratios than HIMU and relative Ba enrichment), consistent with derivation from a HIMU source that contains a small amount of entrapped pelagic sediments; and (3) the enriched mantle II (EM-II), compatible with derivation from a HIMU source that contains a small amount of terrigenous sediments. The use of some incompatible trace element ratios permits an identification of the mantle end-member from which the Bandurrias gabbro was generated. In this sense, the low Th/La ratios (0.11–0.15) are similar to those of the primitive mantle (0.12, Sun and McDonough, 1989), and the Zr/Nb (6.3–7.6), La/Nb (0.76–1.03), Ba/Nb (7.6–17.4), Ba/Th (81–120), Th/Nb (0.09–0.15), K/Nb (370–467), Th/La (0.11–0.15), and Ba/La (10.0–16.9) ratios are typical of an EM-type reservoir.

### 6.3. Petrogenesis

Only sample COY01-06, with Ni contents of 208 ppm and [mg] $=0.64$, can be considered a relatively primary upper mantle partial melt. However, the olivine composition in this rock ($Fo_{75}$) is below the range ($Fo_{88–94}$) expected for primitive magmas derived from a 'normal' upper mantle (Dostal and Owen, 1998).

Trace element modeling can constrain the degree and depth of melting. As we previously noted, $Yb_N$ values $<10$ affirm the presence of garnet as a residual phase in the source. A simple modal batch melting model was used with the gabbro REE concentrations to constrain the degree of melting. Mineral-melt distribution coefficients and the composition of the primitive mantle source were taken from Mertz et al. (2001). We plot the results in Fig. 10, in which the calculated $\approx 3\%$ partial melt fits the composition of sample COY01-06. This low partial melt degree is consistent with the relatively high LILE contents and similar to values obtained by other authors for alkaline gabbros (e.g. Dostal and Owen, 1998; Mertz et al., 2001).

### 6.4. Tectonic setting

The Oligocene period is relatively poorly represented in the geologic record in the central Patagonian Cordillera. With the exception of bimodal volcanism (peralkaline rhyolites and basalts) 100 km north of the studied area (Morata et al., 2003), no plutonic or volcanic rocks of this

Table 7
Whole-rock geochemical analyses of the Bandurrias gabbro, Patagonian Cordillera (46°35′ Lat. S)

| Sample number | Bandurrias Gabbro | | | | | Paso de las Llaves | | | Isla Elena |
|---|---|---|---|---|---|---|---|---|---|
| | COY.01.06 | COY.01.07 | COY.01.10 | COY.01.11 | COY.01.12 | IBA 22 | IBA 23 | IBA 24 | CE94 13A |
| *Major element (wt%)* | | | | | | | | | |
| $SiO_2$ | 45.57 | 46.89 | 47.62 | 45.03 | 46.73 | 51.70 | 52.03 | 50.63 | 48.80 |
| $TiO_2$ | 1.71 | 2.68 | 2.20 | 2.59 | 2.00 | 1.33 | 1.43 | 1.37 | 1.27 |
| $Al_2O_3$ | 14.16 | 16.2 | 16.40 | 16.19 | 17.20 | 18.37 | 18.54 | 19.17 | 19.77 |
| $Fe_2O_3$ | 1.71 | 3.15 | 2.32 | 4.40 | 2.64 | 3.34 | 2.45 | 3.41 | 1.94 |
| FeO | 10.67 | 8.07 | 8.07 | 6.31 | 8.12 | 4.96 | 5.96 | 4.92 | 5.80 |
| MnO | 0.17 | 0.15 | 0.14 | 0.16 | 0.15 | 0.14 | 0.16 | 0.15 | 0.18 |
| MgO | 10.86 | 4.68 | 5.43 | 4.09 | 7.06 | 4.73 | 4.78 | 4.43 | 5.02 |
| CaO | 8.69 | 10.20 | 10.41 | 8.53 | 9.76 | 9.08 | 8.76 | 9.25 | 11.29 |
| $Na_2O$ | 3.33 | 4.29 | 4.19 | 5.32 | 3.87 | 3.40 | 3.19 | 3.88 | 3.20 |
| $K_2O$ | 0.92 | 1.28 | 1.19 | 1.88 | 1.01 | 1.17 | 1.61 | 1.21 | 0.60 |
| $P_2O_5$ | 0.40 | 0.59 | 0.47 | 0.87 | 0.41 | 0.47 | 0.46 | 0.52 | 0.31 |
| LOI | 1.39 | 1.79 | 1.42 | 4.45 | 0.95 | 1.76 | 0.56 | 1.28 | 1.46 |
| Sum | 99.66 | 99.97 | 99.86 | 99.82 | 99.90 | 100.45 | 99.93 | 100.22 | 99.64 |
| *Trace element (ppm)* | | | | | | | | | |
| Ba | 210 | 220 | 240 | 610 | 230 | 420 | 560 | 320 | 130 |
| Th | 2.6 | 2.6 | 2.0 | 5.3 | 2.4 | | | | |
| Nb | 21 | 29 | 22 | 35 | 22 | 8 | 13 | 5 | |
| Sr | 520 | 630 | 620 | 935 | 640 | 800 | 850 | 850 | 385 |
| Zr | 139 | 183 | 166 | 222 | 148 | 109 | 137 | 35 | 136 |
| Y | 18 | 23 | 22 | 27 | 19 | 21 | 24 | 20 | 15 |
| Cr | 200 | 48 | 100 | 7 | 120 | 14 | 29 | 17 | 340 |
| V | 201 | 302 | 228 | 248 | 206 | 250 | 260 | 240 | 136 |
| Ni | 208 | 40 | 66 | 20 | 114 | 13 | 19 | 25 | 51 |
| Co | 47 | 37 | 38 | 32 | 39 | 22 | 29 | 30 | 30 |
| Sc | 20 | 26 | 24 | 13 | 20 | 21 | 25 | 19 | 30 |
| Cu | 40 | 55 | 55 | 40 | 45 | 31 | 22 | 35 | 8 |
| Zn | 113 | 1152 | 100 | 109 | 101 | 127 | 185 | 168 | 72 |
| Hf | 3.6 | 4.6 | 4.2 | 5.0 | 3.7 | | | | |
| *Rare earth element (ppm)* | | | | | | | | | |
| La | 17 | 22 | 19 | 36 | 19 | 24 | 25 | 19 | 5.00 |
| Ce | 34 | 50 | 42 | 79 | 39 | 51 | 57 | 42 | 12.00 |
| Nd | 19 | 26 | 25 | 39 | 22 | 4.17 | 4.8 | 3.28 | 8.00 |
| Sm | 19 | 26 | 25 | 39 | 22 | 30 | 33 | 27 | 2.40 |
| Eu | 4.2 | 6.46 | 5.47 | 8.37 | 5.41 | 5.18 | 5.73 | 5.06 | 1.50 |
| Gd | 1.43 | 2.02 | 1.80 | 2.50 | 1.76 | 1.70 | 1.91 | 1.81 | 3.00 |
| Dy | 4.53 | 6.02 | 5.30 | 7.21 | 5.15 | 5.08 | 5.27 | 5.26 | 3.00 |
| Ho | 3.83 | 5.03 | 4.74 | 5.80 | 4.07 | 4.06 | 4.51 | 3.94 | 0.60 |
| Er | 0.69 | 0.81 | 0.79 | 1.00 | 0.76 | 0.83 | 0.9 | 0.79 | 1.40 |
| Yb | 1.56 | 1.90 | 1.84 | 2.14 | 1.66 | 1.96 | 2.21 | 1.92 | 1.40 |
| Lu | 0.23 | 0.29 | 0.28 | 0.35 | 0.27 | 0.31 | 0.33 | 0.28 | |

Gabbros from the Paso de las Llaves and Isla Santa Elena (Patagonian batholith) from Pankhurst et al. (1999). LOI, loss on ignition at 950 °C.

age have been reported, and in the sedimentary record, only the marine Guadal Formation, assigned to the Late Oligocene–Early Miocene (Frassinetti and Covacecich, 1999) and exposed 160 km southwest of the Bandurrias gabbro in the mountains south of Lago General Carrera (46°30′S), represents the period. The Guadal Formation was deposited in a shallow sea with an Atlantic faunal association and separated by land from coeval marine basins developed along western South America between latitudes 40° and 43°S (Ramos, 1982; Malumián, 1999). Thus, the Guadal Sea appears to have been separated from the Pacific basins, probably by a N-S-trending mountain belt that partially formed during a Paleogene contractional tectonism, which has been well identified in the region of Magallanes approximately 500 km to the south (Biddle et al., 1986). A Middle Eocene–Oligocene hiatus between the Guadal Formation and the underlying Lower Eocene fluvial deposits of the San José Formation may be a reflection of this contractional tectonism, as proposed by Suárez and de la Cruz (2002) and de la Cruz et al. (2003b).

The overall contractional regime in this region during the Cenozoic is punctuated, however, by phases of extensional tectonism, as suggested by the OIB flood basalts that locally extruded during the Eocene and Mio–Pliocene (see De la Cruz et al., 2003) and the Late Oligocene bimodal basalt and peralkaline rhyolites ($29.1 \pm 0.3$ Ma, $^{40}Ar/^{39}Ar$ dating on sanidine) generated by extensional tectonism (Morata et al., 2003). The Bandurrias gabbro, of early Late Oligocene

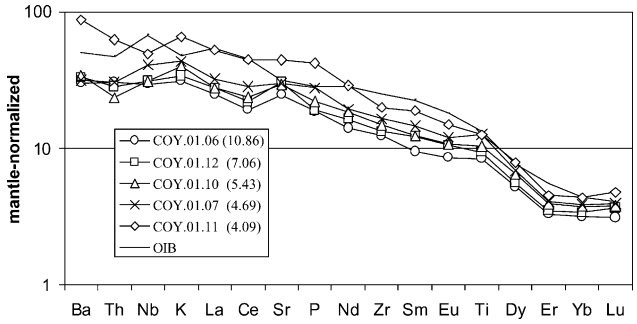


Fig. 8. Primitive mantle normalized spidergram of trace elements of the Bandurrias gabbro. Normalizing values are from Sun and McDonough (1989). In parenthesis, whole-rock MgO wt% content. Average OIB of Sun and McDonough (1989) are plotted.

(ca. 27 Ma) age, probably was emplaced during an extensional or transtensional tectonic setting, according to its geochemical signature.

Farther north, Cenozoic tectonic evolution has differences and similarities with that of the studied region. In the Andean segment in the Lonquimay area (38°–39°S), approximately 800 km to the north, intra-arc extensional or transtensional lacustrine basins developed during the Late Lower–Early Middle Miocene, with a main phase of contractional tectonism in the Late Miocene (Suárez and Emparan, 1995). This tectonic setting has been identified along a wider segment of Chile (38°–42°S) and chronologically extended to include the Late Oligocene (Muñoz et al., 2000; Jordan et al., 2001). Thus, a main tectonic difference existed between the two regions, at least during the Lower and Middle Miocene, with extensional tectonism in the north and contractional tectonism in the south. In turn, during the Late Oligocene, both areas were subject to extensional tectonics.

During the Late Oligocene (ca. 26 Ma), a major reconfiguration of Nazca-South American plate convergence took place. The convergence of the Nazca with the South American plate between 36 and 26 Ma was northeastward and highly oblique to the margin (N10°E; Cande and Leslie, 1986) with a convergence rate of 35 ± 25 mm/a

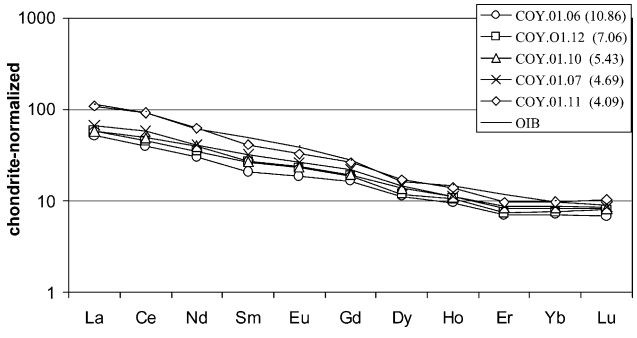


Fig. 9. Chondrite-normalized spidergram of rare earth elements for the Bandurrias gabbro. Normalizing values are from Nakamura (1974). In parenthesis, whole-rock MgO wt% content. Average of OIB of Sun and McDonough (1989) are plotted.

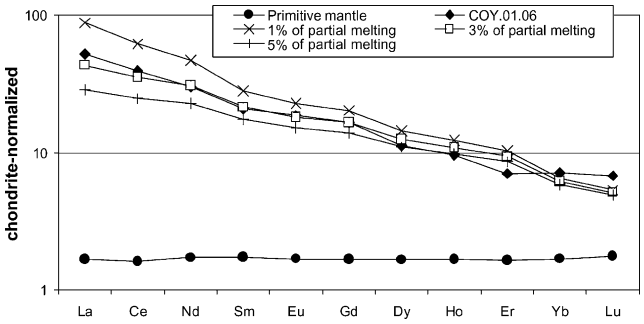


Fig. 10. Batch melting model used to approach the Bandurrias gabbro REE pattern. Primitive mantle composition, mineralogy (66% olivine, 14% orthopyroxene, 15% clinopyroxene, 5% garnet), and mineral/liquid partition coefficients are taken from Mertz et al. (2001). Normalizing values are from Nakamura (1974).

at 40°S in southern Chile (Pardo-Casas and Molnar, 1987). Since approximately 26 Ma, the convergence of these two plates has been approximately N80°E with an average rate of 112 ± 8 mm/a at 40°S (Cande and Leslie, 1986; Pardo-Casas and Molnar, 1987). Where subduction convergence is oblique, such as in the southern South American plate prior to 26 Ma, interplate coupling may cause partitioning of the oblique plate convergence vector into two orthogonal components: trench-orthogonal compression confined to the forearc and present-day plate boundary and trench-parallel strike-slip motion accommodated in the overriding plate (Sanderson and Marchini, 1984; Tikoff and Teyssier, 1994; Arancibia et al., 1999; Cembrano et al., 2002). According to Somoza's (1998) data, in relation to the relative motions of the Nazca and South American plates, a sharp increase in the convergence rate and orthogonality took place during the Late Oligocene (28.3–25.8 Ma).

Thus, the Bandurrias gabbro, dated at ca. 27 Ma with an OIB geochemical signature, may have been emplaced either during the latest phase of slower oblique subduction or at the beginning of the increased rate of near-orthogonal convergence. Current data prevent a valid discrimination, and therefore, any assumptions would be too speculative.

## Acknowledgements

This research was supported by the Chilean National Science Foundation (FONDECYT) Project 1000125. Fieldwork would have been impossible without the assistance of Leonardo Zúñiga (Pituso) and discussions with Dr. Luis Barbero (Universidad de Cádiz, Spain) and Felipe Espinoza (Universidad de Chile, Chile). Dr. Mauricio Belmar (Universidad de Chile, Chile) is thanked for his assistance with the microprobe and SEM analyses. CO thanks the Facultad de Ciencias Físicas y Matemáticas of the Universidad de Chile for a grant during 2002 and CE Project C1I-CT930033. Revision, comments, and suggestions by R.J. Pankhurst, J. Muñoz, and an anonymous reviewer improved a previous version of this manuscript.

## References


Arancibia, G., Cembrano, J., Lavenu, A., 1999. Transpresión dextral y partición de la deformación en la Zona de Falla Liquiñe-Ofqui, Aisén, Chile (44–45°S). Revista Geológica de Chile 26, 3–22.

Azambre, B.G., Rossy, M., Albarede, F., 1992. Petrology of the alkaline magmatism from the Cretaceous North-Pyrenean Rift Zone (France and Spain). European Journal of Mineralogy 4, 813–834.

Baker, P.E., Rea, W.J., Skarmeta, J., Caminos, R., Rex, D.C., 1981. Igneous history of the Andean Cordillera and Patagonian Plateau around latitude 46°S. Philosophical Transaction of the Royal Society of London A303, 105–149.

Biddle, K., Uliana, R., Mitchum, R., Fitzgerald, M., Wright, R., 1986. The stratigraphic and structural evolution of the central and eastern Magallanes basin, southern South America, in: Allen, P.A., Homewood, P. (Eds.), Foreland Basins, International Association of Sedimentologists, Special Publications, 8, pp. 41–61.

Brown, G.E., 1982. Olivines and silicate spinels, in: Ribbe, P.H. (Ed.), Orthosilicates, Review in Mineralogy, Mineral Society American, 5, pp. 275–381.

Bruce, R.M., Nelson, E.P., Weaver, S.G., Lux, D.R., 1991. Temporal and spatial variations in the southern Patagonian batholith; Constraints on magmatic arc development, in: Harman, R.S., Rapela, C.W. (Eds.), Andean Magmatism and its Tectonic Setting, Geological Society of America, Special Paper, 265, pp. 1–12.

Busteros,A., Lapido, O., 1983. Rocas básicas en la vertiente noroccidental de la Meseta del Lago Buenos Aires, Provincia de Santa Cruz. Asociación Geológica Argentina Revista XXXVII (3–4), 427–436.

Cande, S.C., Leslie, R.B., 1986. Late Cenozoic tectonics of southern Chile trench. Journal of Geophysical Research 91B, 471–496.

Cembrano, J., Lavenu, A., Reynolds, P., Arancibia, G., López, G., Sanhueza, A., 2002. Late Cenozoic transpressional ductile deformation north of the Nazca–South America–Antartica triple junction. Tectonophysics 354, 289–314.

Chambers, A.D., Brown, P.E., 1995. The Lilloise intrusion East Greenland: fractionation of a hydrous alkali picritic magma. Journal of Petrology 36, 933–963.

Coulon, C., Megartsi, M., Fourcade, S., Maury, R.C., Bellon, H., Louni-Hacini, A., Cotten, J., Coutelle, A., Hermitte, D., 2002. Post-collisional transition from calc-alkaline to alkaline volcanism during the Neogene in Oranie (Algeria): magmatic expression of a slab breakoff. Lithos 62, 87–110.

De la Cruz, R., Suárez, M., Belmar, M., Quiroz, D., Bell, M. 2004. Mapa geológico Coyhaique-Balmaceda, escala 1:100.000, Servicio Nacional de Geología y Minería.

De la Cruz, R., Suárez, M., Morata, D., Espinoza, F., Troncoso, A., 2003. El Cenozoico del Lago General Carrera, Aysén, Chile (46°30′–47°15′s): estratigrafía y tectónica. X Congreso Geológico Chileno, Concepción (Octubre).

Demant, A., Hervé, F., Pankhurst, R.J., Suárez, M., 1996. Geochemistry of Early Tertiary back-arc basalts from Aysén, southern Chile (44°–46°S): geodynamic implications. Third ISAG, St Malo (France) 1996, 555–558 (extended abstract).

D'Orazio, M., Agostini, S., Innocenti, F., Haller, M.J., Manetti, P., Mazzarini, F., 2001. Slab window-related magmatism from southernmost South America: The Late Miocene mafic volcanics from the Estancia Glencross Area (∼52°S Argentina-Chile). Lithos 57, 67–89.

Dostal, J., Owen, J.V., 1998. Cretaceous alkaline lamprophyres from northeastern Czech Republic: Geochemistry and petrogenesis. Geologische Rundschdau 87, 67–77.

Droop, G.T.R., 1987. A general equation for estimating $Fe^{3+}$ concentrations in ferromagnesian silicates and oxides from microprobe analysis using stoichiometric criteria. Mineralogical Magazine 55, 431–435.

Flint, S.S., Prior, D.J., Agar, S.M., Turner, P., 1994. Stratigraphic and structural evolution of the Tertiary Cosmelli Basin and its relationship to the Chile triple junction. Journal of the Geological Society of London 151, 251–268.

Flynn, J.J., Novacek, M.J., Dodson, H.E., Frassinetti, D., McKenna, M.C., Norell, M.A., Sears, K.E., Swisher, C.C., Wyss, A.R., 2002. A new fossil mammal assemblage from the southern Chilean Andes: implications for geology, geochronology, and tectonics. Journal of South American Earth Sciences 15, 285–302.

Frassinetti, D., Covacecich, V., 1999. Invertebrados fósiles marinos de la Formación Guadal (Oligoceno Superior-Mioceno Inferior) en Pampa Castillo, región de Aysén, Chile. Servicio Nacional de Geología y Minería, Boletín 51, 96pp.

Gorring, M.L., Kay, S.M., 2001. Mantle processes and sources of Neogene slab window magmas from Southern Patagonia, Argentina. Journal of Petrology 42, 1067–1094.

Green, T.H., Ringwood, A.E., 1968. Genesis of the calc-alkaline igneous rock suite. Contributions to Mineralogy and Petrology 18, 105–162.

Griffiths, J.B., Gruau, G., Cornen, G., Azambre, B., Magé, J., 1997. Continental lithospheric contribution to alkaline magmatism: isotopic (Nd, Sr, Pb) and geochemical (REE) evidence from Serra de Monchique and Mount Ormonde complexes. Journal of Petrology 38, 115–132.

Haschke, M.R., Scheuber, E., Günter, A., Reutter, K.-J., 2002. Evolutionary cycles during the Andean orogeny: repeated slab breakoff and flat subduction?. Terra Nova 14, 49–55.

Hervé, F., Aguirre, L., Sepúlveda, V., Morata, D., 1999. Contrasting geochemistry and metamorphism of pillow basalts in metamorphic complexes from Aysén, S. Chile. Journal of South American Earth Sciences 12, 379–388.

Hole, M.J., Saunders, A.D., Rogers, G., Sykes, M.A., 1995. The relationship between alkaline magmatism, lithospheric extension and slab window formation along continental destructive plate margins, in: Smellie, J.L. (Ed.), Volcanism Associated with Extension at Consuming Plate Margins, Geological Society Special Publication, 81, pp. 265–285.

Jordan, T., Burns, W., Veiga, R., Pángaro, F., Copeland, P., Kelley, S., Mpodozis, C., 2001. Extension and basin formation in the southern Andes caused by increased convergence rate: a mid-Cenozoic trigger for the Andes. Tectonics 20, 308–324.

Le Bas, M.J., 1962. The role of aluminium in igneous clinopyroxene with relation to their parentage. American Journal of Sciences 260, 267–268.

Leake, B., Woolley, A., Arps, C., Birch, W., Gilbert, M., Grice, J., Hawthorne, F., Akira, K., Kisch, H., Krivovichev, V., Linthout, K., Laird, J., Mandarino, J., Maresch, W., Nickel, E., Rock, N., Schumacher, J., Smith, D., Stephenson, N., Ungaretti, L., Whittaker, E., Guo, Y., 1997. Nomenclature of amphiboles: report of the subcommittee on amphiboles of the international mineralogical association, commission on new minerals and mineral names. Canadian Mineralogist 35, 219–246.

Malumián, N., 1999. La Sedimentación y el volcanismo terciarios en la Patagonia extraandina, in: Caminos, R. (Ed.), Geología Argentina. Instituto de Geología y Recursos Minerales, Anales, pp. 557–612.

Mertz, D.F., Weinrich, A.J., Sharp, W.D., Renne, P.R., 2001. Alkaline intrusions in a near-trench setting, Franciscan complex, California: constraints from geochemistry, petrology, and $^{40}Ar/^{39}Ar$ chronology. American Journal of Sciences 301, 877–911.

Morata, D., Higueras, P., 1996. Analcimas en lavas alcalinas del Sinclinal de Almadén, ¿Origen primario o secundario? Implicaciones petrogenéticas. Boletín de la Sociedad Española de Mineralogía 19, 27–37.

Morata, D., de la Cruz, R., Suárez, M., Demant, A., 2000. Mantle xenoliths and xenocrysts in the Late Paleocene Patagonian continental flood basalts from Aysen, Chile. IX Congreso Geológico Chileno Actas 2, 226–229.

Morata, D., Barbero, L., Suárez, M., de la Cruz, R., 2002. Early Pliocene magmatism and high exhumation rates in the Patagonian Cordillera (46°40′S): K–Ar and fission track data. Fifth International Symposium on Andean Geodynamics, Actas, pp. 433–436.

Morata, D., Demant, A., de la Cruz, R., Barbero, L., Suárez, M., 2003. Late Oligocene peralkaline rhyolites related with bimodal volcanism in the Eastern Patagonian Cordillera evidences for an incipient back-arc extensional setting?. X Congreso Geológico Chileno, Concepción (Octubre) 2003.

Morimoto, N., Fabries, J., Fergusson, A.K., Guizbourg, I.D., Ross, M., Seifert, F.A., Zussman, J., Aoki, K., Gottardi, G., 1988. Nomenclature of pyroxenes. American Mineralogist 173, 1123–1133.

Muñoz, J., Troncoso, R., Duhart, P., Crignola, P., Farmer, L., Stern, C.R., 2000. The relation of the mid-Tertiary coastal magmatic belt in south-central Chile to the late Oligocene increase in plate convergence rate. Revista Geológica de Chile 27, 177–203.

Nakamura, N., 1974. Determination of REE, Ba, Mg, Na and K in carbonaceous and ordinary chondrites. Geochimica et Cosmichimica Acta 38, 757–775.

Ngounouno, I., Moreau, C., Déruelle, B., Demaiffe, D., Montigny, R., 2001. Pétrologie du complexe alcalin sous-saturé de Kokoumi (Cameroun). Bulletin de la Societé géologique de la France 172, 675–686.

Niemeyer, H., Skarmeta, J., Fuenzalida, R., Espinosa, W., 1984. Hojas Península de Taitao y Puerto Aysén. Servicio Nacional de Geología y Minería, Carta Geológica de Chile, Nos. 60–61, pp. 80 (+1 mapa).

Pankhurst, R.J., Leat, P.T., Sruoga, P., Rapela, C.W., Márquez, M., Storey, B.C., Riley, T.R., 1998. The Chon-Aike province of Patagonia and related rocks in West Antarctica: a silicic large igneous province. Journal of Volcanology and Geothermal Research 81, 113–136.

Pankhurst, R.J., Weaver, S.D., Hervé, F., Larrondo, P., 1999. Mesozoic-Cenozoic evolution of the North Patagonian Batholith in Aysén, southern Chile. Journal of the Geological Society of London 156, 673–694.

Pankhurst, R.J., Riley, T.R., Fanning, C.M., Kelley, S.P., 2000. Episodic silicic volcanism in Patagonia and the Antarctic Peninsula: Chronology and magmatism associated with the break-up of Gondwana. Journal of Petrology 41, 605–625.

Pardo-Casas, F., Molnar, P., 1987. Relative motions of the Nazca (Farallon) and South American plates since Late Cretaceous times. Tectonics 6, 233–248.

Ramos, V., 1982. Las ingresiones Pacíficas del terciario del norte de la Patagonia (Argentina): actas III Congreso geológico Chileno. Tomo I 1982;, A-262–288.

Richard, L.R., Clarke, D.B., 1990. AMPHIBOL: a program for calculating structural formulae and for classifying and plotting chemical analyses of amphiboles. American Mineralogist 75, 421–423.

Sanderson, D., Marchini, W., 1984. Transpression. Journal of Structural Geology 6, 449–458.

Shervais, J.W., 1982. Ti–V plots and the petrogenesis of modern and ophiolitic lavas. Earth and Planetary Science Letters 59, 101–118.

Somoza, R., 1998. Updated Nazca (Farallon)-South America relative motions during the last 40 My: implications for mountain building in the central Andean region. Journal of South American Earth Sciences 11, 211–215.

Stern, C.R., Frey, F.A., Kiyoto, F., Zartman, R.E., Peng, Z., Kyser, T.K., 1990. Trace-element and Sr, Nd, Pb, and O isotopic composition of Pliocene and Quaternary alkali basalts of the Patagonian Plateau lavas of southernmost South America. Contributions to Mineralogy and Petrology 104, 294–308.

Stern, C.R., Muñoz, J., Troncoso, R., Duhart, P., Crignola, P., Farmer, G.L., 2000. The Mid-Tertiary coastal magmatic belt in south-central Chile: The westernmost portion of an extensional event related to late Oligocene changes in plate convergence rate and subduction geometry. 9° Congreso Geológico Chileno Actas 2, 693–696.

Suárez, M., de la Cruz, R., 2001. Jurassic to Miocene K–Ar dates from eastern central Patagonian Cordillera plutons, Chile (45°–48°S). Geological Magazine 138, 53–66.

Suárez, M., de la Cruz, R., 2002. Stratigraphic discontinuities in the Meso–Cenozoic of eastern Aysén, Chile (44°–47°S). XV Congreso geológico Argentino, Tomo I 2002, 706–710 (El Calafate).

Suárez, M., Emparán, C., 1995. The stratigraphy, geochronology and paleophysiography of a Miocene fresh-water interact basin, southern Chile. Journal of South American Earth Sciences 8, 17–31.

Suárez, M., de la Cruz, R., Bell, M., 1996. Estratigrafía de la región de Coyhaique (latitud 4S–46°S); Cordillera Patagónica, Chile. XIII Congreso Geológico Argentino y III Congreso de Exploración de Hidrocarburos Actas I, 575–590.

Suárez, M., Demant, A., de la Cruz, R., 1999. Volcanismo calcoalcalino en W Provincia Chon Aike: Grupo Ibáñez, Jurásico Superior-Cretácico Inferior temprano, Cordillera Patagónica de Aysén, Chile (45°30′–46°30′S). Actas IV Congreso Geológico Argentino, Salta II 1999, 186–189.

Suárez, M., de la Cruz, R., Troncoso, A., 2000. Tropical/subtropical upper Paleocene–lower Eocene fluvial deposits in eastern central Patagonia, Chile (46°45′S). Journal of South American Earth Sciences 13, 527–536.

Sun, S., McDonough, W., 1989. Chemical and isotopic systematic of oceanic basalt: Implications for mantle composition and processes, Magmatism in the Ocean Basins, Geological Society Special Publications, 42, pp. 313–345.

Tikoff, B., Teyssier, C., 1994. Strain modelling of displacement-field partitioning in transpresional orogens. Journal of Structural Geology 16, 1575–1588.

Vargas, G., Hervé, F., 1994. Emplazamiento hipabisal mioceno tardío del stock de Paso de las Llaves en la región de tras arco, Aysén. Comunicaciones 46, 3–16.

Weaver, B.L., 1991. Trace element evidence for the origin of ocean-island basalts. Geology 19, 123–126.

Weaver, S.G., Bruce, R., Nelson, E.P., Brueckner, H.K., Lehuray, A.P., 1990. The Patagonian batholith at 48°S latitude, Chile; Geochemical and isotopic variations, in: Kay, S.M., Rapela, C.W. (Eds.), Plutonism from Antarctica to Alaska, Geological Society of America Special Paper, 241, pp. 33–50.

Wedepohl, K.H., Gohn, E., Hartmann, G., 1994. Cenozoic alkali basaltic magmas of western Germany and their products of differentiation. Contributions to Mineralogy and Petrology 115, 253–278.

Welkner, D., Godoy, E., Bernhardt, H.-J., 2002. Peralkaline rocks in the Late Cretaceous del Salto Pluton, Eastern Patagonian Andes, Aysén, Chile (47°35′S). Revista Geológica de Chile 29, 3–15.

Wilson, M., Downes, H., 1991. Tertiary-Quaternary extension-related alkaline magmatism in Western and Central Europe. Journal of Petrology 32, 811–849.

Wilson, M., Downes, H., Cebriá, J.M., 1995. Contrasting fractionation trends in coexisting continental alkaline magma series; Cantal, Massif Central, France. Journal of Petrology 36, 1729–1735.